Electronic Supplementary Information

Carbon fibers with infiltrated TiO_2 nanocrystalline layers: photocatalytic performance

Pavan Kumar Chennam[a], Martina Rihova[a], Susan Azpeitia[b], Marcela Sepúlveda[a,c], Martin Kachlík[a], Miloslav Pouzar[c], Veronika Čičmancová[c], Karel Maca[a], Mato Knez[b,d], Jan M. Macak[a,c]*

[a] Central European Institute of Technology, Brno University of Technology, Purkynova 123, 61200 Brno, Czech Republic

[b] CIC nanoGUNE BRTA, Tolosa Hiribidea 76, E-20018 Donostia/San Sebastian, Spain

[c] Center of Materials and Nanotechnologies, Faculty of Chemical Technology, University of Pardubice, Nam. Cs. Legii 565, 53002 Pardubice, Czech Republic.

[d] Ikerbasque, Basque Foundation for Science, Plaza Euskadi 3, E-48009 Bilbao, Spain

*Corresponding author: J.M. Macak, E-mail: jan.macak@upce.cz

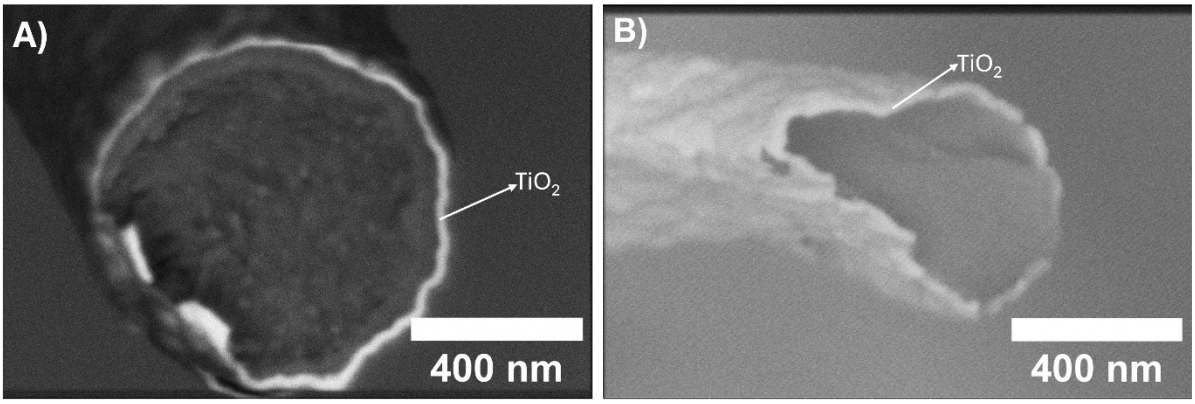

Figure S1: Cross-sectional SEM images, acquired with a mirror detector, enabling to visualize the TiO_2 layers infiltrated within (A) PAN fibers and (B) CFs.

Figure S1 shows the cross-sectional SEM images of PAN fibers and CFs fibers infiltrated with TiO_2 layers using a mirror detector. This particular mirror detector enhances the material contrast and allows the TiO_2 to be distinguished from the fiber core. The TiO_2 appears as a uniform layer surrounding the fiber surface, supporting the idea that the TiO_2 coating is a conformal nanocrystalline layer rather than a nanoparticulate layer. The presence of the coating around the fiber surface is an indication that the deposition process was effective at producing continuous layers of TiO_2.

Figure S2 shows XRD patterns of neat PAN fibers and PAN fibers infiltrated with TiO_2 (PAN@TiO_2) using various VPI cycles ranging from 40c to 160c. PAN shows reflections at ~ $2\theta = 17°$ (100) and near 29-30° (110). For all PAN@TiO_2 samples, the signature of PAN is maintained. There are no observable reflections associated with the crystalline TiO_2 (e.g. anatase (101) ~25.7°).

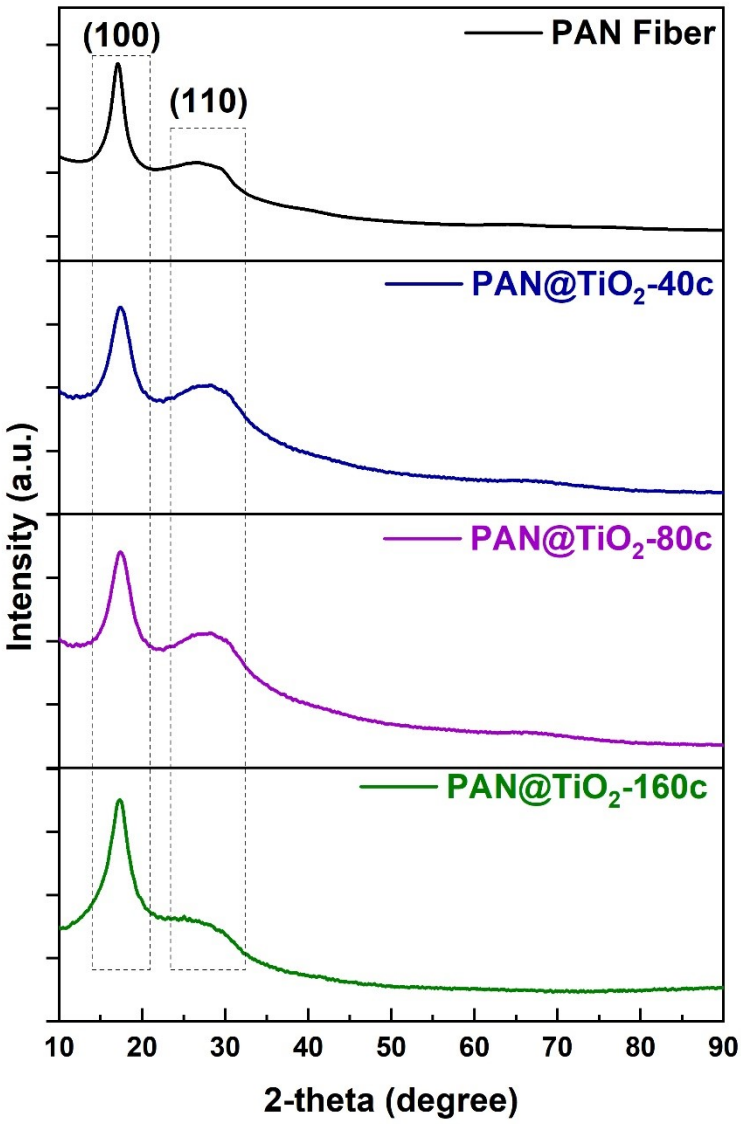

Figure S2: XRD patterns of PAN@TiO_2 (prepared using 40c, 80c and 160c VPI cycles to incorporate TiO_2 into PAN.

XPS analyses

The survey XPS spectrum of CFs@TiO_2 (sample -160c) contains signals from C1s, N1s, Ti2p and O1s (Figure S3). Figure S4 shows high-resolution XPS spectra around C 1s, N 1s, O 1s, and Ti 2p. The binding energy of all XPS spectra was calibrated by referencing the C–C component of the adventitious carbon C 1s peak to 284.8 eV. Color coding remains the same for clarity: red = experimental raw spectrum; blue = best-fit envelope from peak deconvolution; black = background function that was used for fitting. Color coding allows for easy distinction

between the measured signal, model, and baseline. Figure S4a displays the C1s spectra for (sample-160c). The curve fitting revealed four peak contributions at 284.6 eV, 285.6 eV, 287 eV, and 289 eV, which were attributed to C-C [1], C-O/C-N [2], C-O [3], and C=O [4]. Figure S4b shows the N1s spectra for (sample-160c). The curve fitting showed three peak components at 396 eV, 396.6 eV, and 399.8 eV. Several studies revealed XPS peaks in the region (396-403 eV), which are typical of N-doped TiO_2 [2],[5], [6], [7]. The nitrogen peaks at 396.0–397.0 eV are ascribed to substitutional nitrogen (β-N state), with the typical binding energy (BE) for Ti in TiN [5], [8]. Typically, peaks at 399.0–403.0 eV are attributed to chemisorbed nitrogen or interstitial nitrogen (γ-N state) [2], [6]. Therefore, the XPS results can be used to infer that nitrogen is not only effectively implanted in the structure, but it is also present in a chemically bonded state, as indicated by this form of nitrogen being the active doping species. The O1s spectra for sample (160c) are shown in Figure S4c. The curve fitting provided three components: 530.2 eV, 532.5 eV, and 534.1 eV. The Ti–O bond in the TiO_2 lattice is responsible for the most significant oxygen peak at 530.2 eV [2]. Other peaks at 532.5 eV and 534.1 eV were ascribed to C=O [9] and C-O [10], [11] bonds, respectively. Figure S4d shows the high-resolution XPS spectra of Ti2p, which have been deconvoluted into four peaks at 457.4, 458.9, 462.6, and 464.5 eV, respectively. The peaks at 457.4 eV ($2p_{3/2}$) and 462.6 eV ($2p_{1/2}$) could be attributed to Ti(III). The peaks at 458.9 eV ($2p_{3/2}$) and 464.5 eV ($2p_{1/2}$) have been correlated to Ti(IV) (TiO_2) [12].

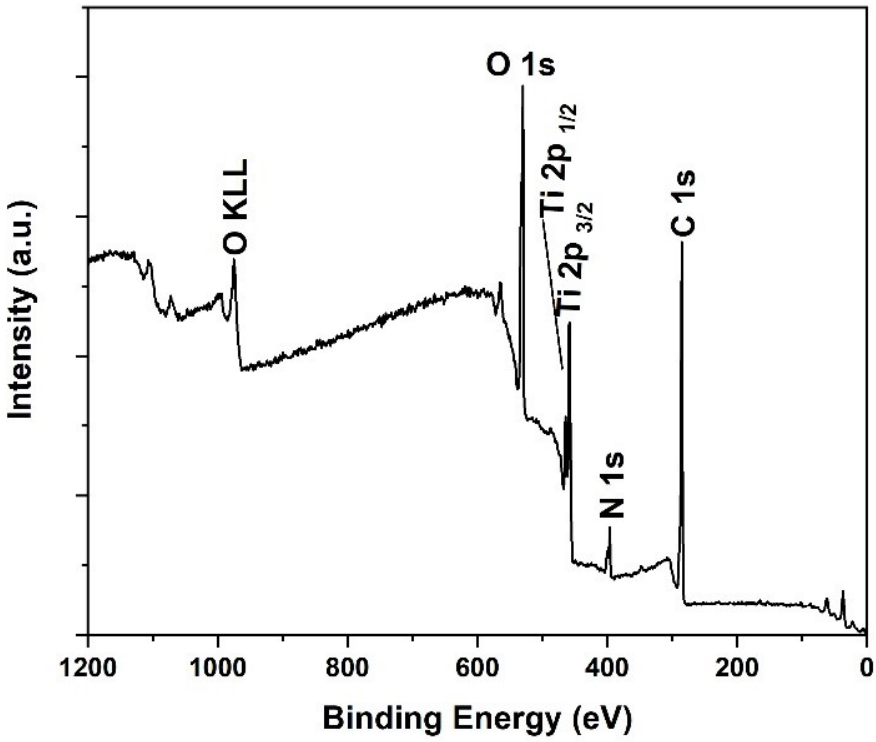

Figure S3: XPS survey spectrum of CFs@TiO_2-160c.

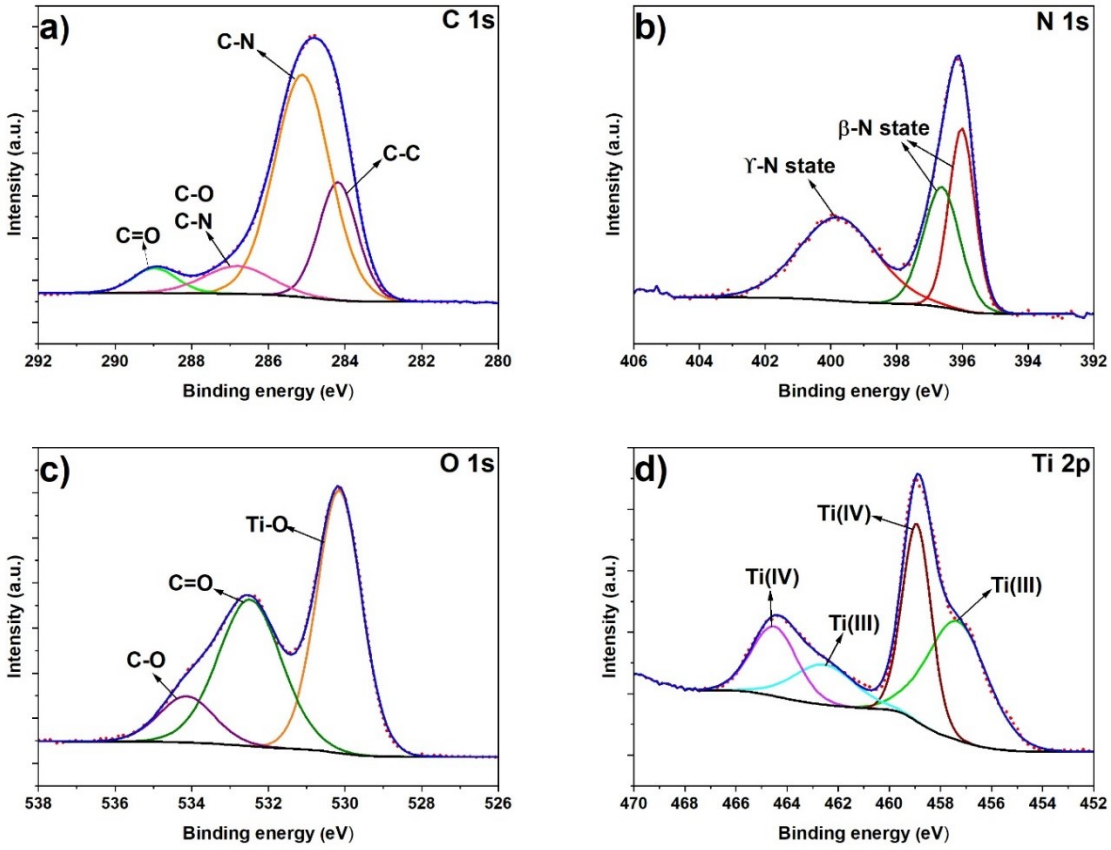

Figure S4: High-resolution XPS spectra of CFs@TiO_2-160c: a) C 1s, b) N 1s, c) O 1s, d) Ti 2p peaks.

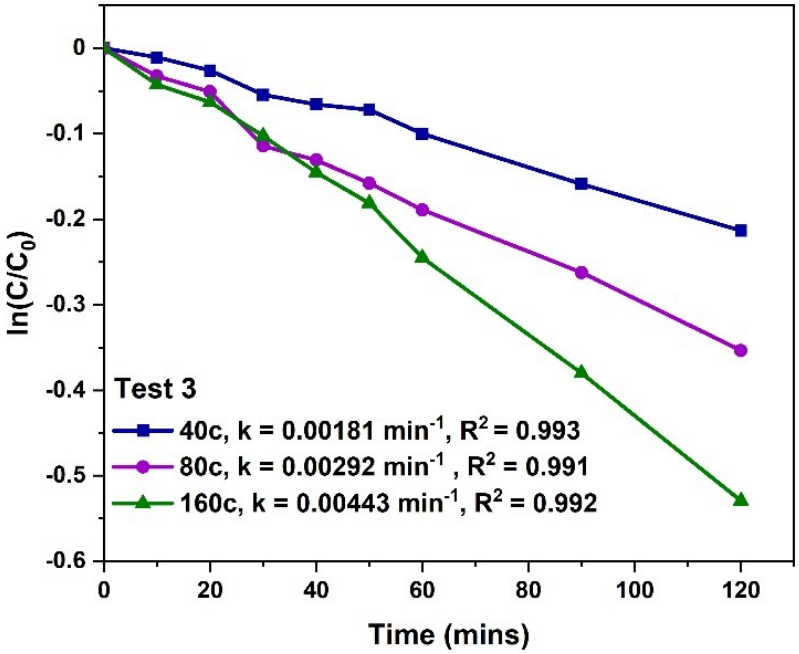

Figure S5: Photocatalytic degradation kinetics curves of MB for CFs@TiO_2 (test 3)

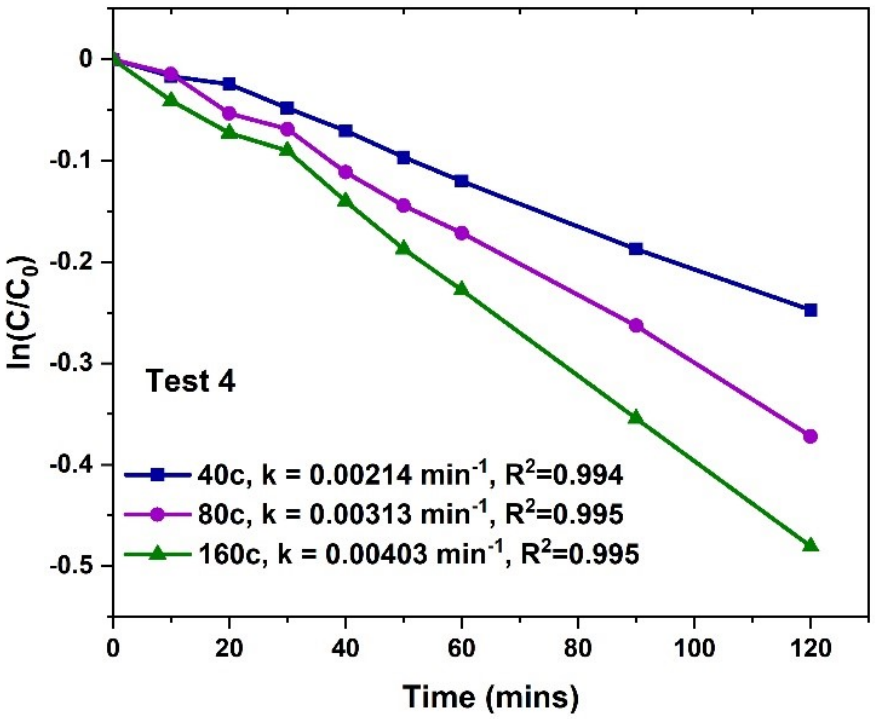

Figure S6: Photocatalytic degradation kinetics curves of MB for CFs@TiO_2 (test 4).

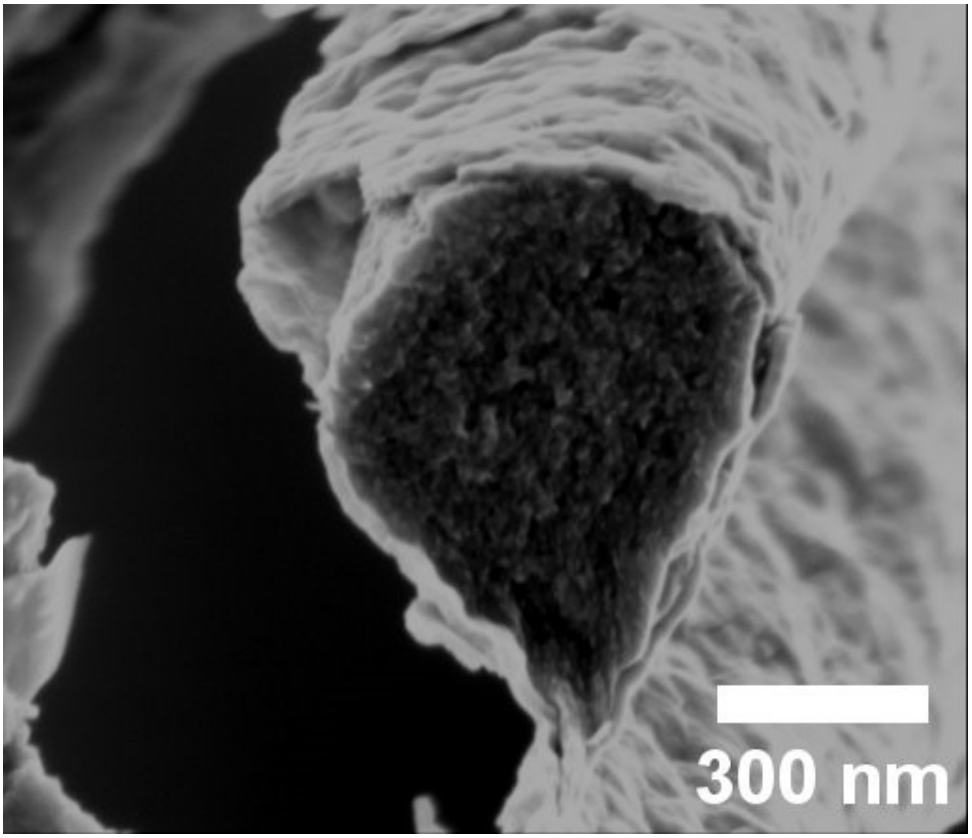

Figure S7: Cross-sectional SEM image of CFs@TiO_2 fibers -160c after photocatalysis.

Table S1: Carbon-based TiO_2 photocatalysts prepared by various synthesis routes with their pseudo-first-order reaction rate constants

Synthesis route	**Photocatalyst**	**Highest rate constant (K_{app})**	**References**
Sol-gel spin coating	TiO_2/CNT	0.0097 min^{-1}	[13]
Electrospinning + high temperature treatment	TiO_2-CNF	0.012 min^{-1}	[14]
Solvothermal method	C-TiO_2	0.01205 min^{-1}	[15]
ALD	Pt@TiO_2@CNTs	0.0158 min^{-1}	[16]
Sol gel	TiO_2/PAC	0.01682 min^{-1}	[17]
hydrothermal method	C-TiO_2	0.0183 min^{-1}	[18]
hydrothermal treatment	TiO_2/AC	0.0191 min^{-1}	[19]
Sol gel + calcination	TiO_2/CF	0.03289 min^{-1}	[20]
hydrothermal method	TiO_2NRs0.3/CC	0.0332 min^{-1}	[21]
Dip coating	CFs@TiO_2- 0.025M	0.20931 min^{-1}	[22]
VPI	CFs@TiO_2-160c	0.00424 min^{-1}	**Our study**

References

[1] G. Greczynski, L. Hultman, Self-consistent modelling of X-ray photoelectron spectra from air-exposed polycrystalline TiN thin films, Appl Surf Sci 387 (2016) 294–300. https://doi.org/10.1016/J.APSUSC.2016.06.012.

[2] M. Pisarek, M. Krawczyk, M. Hołdyński, W. Lisowski, Plasma Nitriding of TiO2 Nanotubes: N-Doping in Situ Investigations Using XPS, ACS Omega 5 (2020) 8647–8658. https://doi.org/10.1021/acsomega.0c00094.

[3] R. Jribi, E. Barthel, H. Bluhm, M. Grunze, P. Koelsch, D. Verreault, E. Søndergård, Ultraviolet Irradiation Suppresses Adhesion on TiO2, The Journal of Physical Chemistry C 113 (2009) 8273–8277. https://doi.org/10.1021/jp809607b.

[4] C. Gadois, J. Światowska, S. Zanna, P. Marcus, Influence of Titanium Surface Treatment on Adsorption of Primary Amines, The Journal of Physical Chemistry C 117 (2013) 1297–1307. https://doi.org/10.1021/jp306786w.

[5] J.M. Macak, A. Ghicov, R. Hahn, H. Tsuchiya, P. Schmuki, Photoelectrochemical properties of N-doped self-organized titania nanotube layers with different thicknesses, J Mater Res 21 (2006) 2824–2828.

[6] A. Ghicov, J.M. Macak, H. Tsuchiya, J. Kunze, V. Haeublein, L. Frey, P. Schmuki, Ion implantation and annealing for an efficient N-doping of TiO2 nanotubes, Nano Lett 6 (2006) 1080–1082.

[7] M. Sathish, B. Viswanathan, R.P. Viswanath, C.S. Gopinath, Synthesis, Characterization, Electronic Structure, and Photocatalytic Activity of Nitrogen-Doped TiO2 Nanocatalyst, Chemistry of Materials 17 (2005) 6349–6353. https://doi.org/10.1021/cm052047v.

[8] C. Di Valentin, E. Finazzi, G. Pacchioni, A. Selloni, S. Livraghi, M.C. Paganini, E. Giamello, N-doped TiO2: Theory and experiment, Chem Phys 339 (2007) 44–56. https://doi.org/10.1016/J.CHEMPHYS.2007.07.020.

[9] R. Huang, J. Zhang, Z. Dong, H. Lin, S. Han, Reticulated TiO2-Modified Carbon Fiber Enabling as a Supercapacitor Electrode Material for Photoelectric Synergistic Charge Storage, Energy & Fuels 36 (2022) 9261–9271. https://doi.org/10.1021/acs.energyfuels.2c02078.

[10] Y.H. Seon, R. Saroha, J.S. Cho, Hierarchically porous N-doped C nanofibers comprising TiO2 quantum dots and ZIF-8-derived hollow C nanocages as ultralight interlayer for stable Li–S batteries, Compos B Eng 237 (2022) 109856. https://doi.org/10.1016/J.COMPOSITESB.2022.109856.

[11] H.O. Seo, C.W. Sim, K.D. Kim, Y.D. Kim, J.H. Park, B.C. Lee, K.H. Lee, D.C. Lim, Influence of High-energy electron-beam on photocatalytic activity of TiO2 films on carbon-fiber deposited by atomic layer deposition, Radiation Physics and Chemistry 81 (2012) 290–294. https://doi.org/10.1016/J.RADPHYSCHEM.2011.11.026.

[12] A. Grube, A.A. Shamsabadi, M.D. Firouzjaei, S.I.G.P. Mohamed, L. Hilger, M. Elliott, K. McKenzie, M. Bavarian, Emperor's new clothes: Novel textile-based supercapacitors using sheep wool fiber as electrode substrate, Nano Trends 3 (2023) 100014. https://doi.org/10.1016/J.NWNANO.2023.100014.

[13] H.K. Sharma, B.P. Singh, S.K. Sharma, CNT-TiO2 nanocomposite thin films enhanced photocatalytic degradation of methylene blue, Hybrid Advances 5 (2024) 100152. https://doi.org/10.1016/J.HYBADV.2024.100152.

[14] C.H. Kim, B.H. Kim, K.S. Yang, TiO2 nanoparticles loaded on graphene/carbon composite nanofibers by electrospinning for increased photocatalysis, Carbon N Y 50 (2012) 2472–2481. https://doi.org/10.1016/J.CARBON.2012.01.069.

[15] J. Matos, A. García, L. Zhao, M.M. Titirici, Solvothermal carbon-doped TiO2 photocatalyst for the enhanced methylene blue degradation under visible light, Appl Catal A Gen 390 (2010) 175–182. https://doi.org/10.1016/J.APCATA.2010.10.009.

[16] S.-Y. Liao, Y.-C. Yang, S.-H. Huang, J.-Y. Gan, Synthesis of Pt@TiO2@CNTs Hierarchical Structure Catalyst by Atomic Layer Deposition and Their Photocatalytic and Photoelectrochemical Activity, Nanomaterials 7 (2017). https://doi.org/10.3390/nano7050097.

[17] X.-P. Guo, P. Zang, Y.-M. Li, D.-S. Bi, TiO2-Powdered Activated Carbon (TiO2/PAC) for Removal and Photocatalytic Properties of 2-Methylisoborneol (2-MIB) in Water, Water (Basel) 13 (2021). https://doi.org/10.3390/w13121622.

[18] G.B. Markad, S. Kapoor, S.K. Haram, P. Thakur, Metal free, carbon-TiO2 based composites for the visible light photocatalysis, Solar Energy 144 (2017) 127–133. https://doi.org/10.1016/J.SOLENER.2016.12.025.

[19] A. Farghaly, E. Maher, A. Gad, H. El-Bery, Synergistic photocatalytic degradation of methylene blue using TiO2 composites with activated carbon and reduced graphene oxide: a kinetic and mechanistic study, Appl Water Sci 14 (2024) 228. https://doi.org/10.1007/s13201-024-02286-0.

[20] H. Cheng, W. Zhang, X. Liu, T. Tang, J. Xiong, Fabrication of titanium dioxide/carbon fiber (TiO2/CF) composites for removal of methylene blue (MB) from aqueous solution with enhanced photocatalytic activity, J Chem 2021 (2021) 9986158.

[21] S.R. AR, K.B. Ansari, S.J. Lee, N. Salunke, Synergistic Integration of TiO2 Nanorods with Carbon Cloth for Enhanced Photocatalytic Hydrogen Evolution and Wastewater Remediation, Catalysts 15 (2025). https://doi.org/10.3390/catal15100961.

[22] P. Kumar Chennam, M. Sepúlveda, M. Rihova, M. Alijani, M. Kachlík, R. Zazpe, D. Pavlinak, K. Maca, J.M. Macak, Carbon fibers decorated with TiO2 nanoparticles for photocatalytic degradation of methylene blue dye, Frontiers in Nanotechnology 6 (2024). https://www.frontiersin.org/journals/nanotechnology/articles/10.3389/fnano.2024.1483917.